Pressure Swing Assisted Desorption for Atmospheric Water Collection

by

Haeri Kim

Submitted to the Department of Mechanical Engineering
in partial fulfillment of the requirements for the degree of

BACHELOR OF SCIENCE

at the

MASSACHUSETTS INSTITUTE OF TECHNOLOGY

May 2024

Authored by: Haeri Kim
Department of Mechanical Engineering
May 10, 2024

Certified by: Gang Chen
Professor of Mechanical Engineering
Thesis Supervisor

Accepted by: Kenneth Kamrin
Associate Professor of Mechanical Engineering
Undergraduate Officer

Pressure Swing Assisted Desorption for Atmospheric Water Collection

by

Haeri Kim

Submitted to the Department of Mechanical Engineering
on May 10, 2024 in Partial Fulfillment of the
Requirements for the Degree of

Bachelor of Science in Mechanical Engineering

ABSTRACT

Ensuring water equity is an urgent and challenging issue in the light of climate change, global conflict, and socioeconomic disparities. Atmospheric water harvesting provides a promising option to collect water from the air, even in considerably dry conditions (RH < 40%), expanding the reach of this application to areas that would be particularly prone to clean water scarcity. The MIT Device Research Lab is developing a device for such applications that would be capable of producing drinkable water in even extremely dry environments. Current methods of atmospheric water harvesting focus on thermal desorption, where heat is applied to release the water vapor from the sorbent. Another method worth exploring is utilizing pressure swings to release this water vapor, and seeing how a combined method of thermal and depressurized desorption would affect the efficiency of this device. An initial MATLAB model showed that the methods, in order of slowest to fastest, should be (1) solely pressure swing desorption, (2) solely temperature swing desorption, and (3) the combined method using simultaneous pressure and temperature swings. The results from the experiment using the MOF UiO-66 as the sorbent showed that the combined procedure would indeed be the fastest, potentially twice as fast as a purely thermal desorption method and five times faster than a purely depressurized desorption method. The next step following this project would be the assembly of a vacuum-grade enclosure in which a small scale test unit of the device the MIT DRL is developing. A detailed design and brief procedure is included in the final section of this thesis.

Thesis supervisor: Gang Chen
Title: Professor of Mechanical Engineering

ACKNOWLEDGMENTS

Thank you Dr. David Keisar for your constant guidance, patience, and mentorship. Thank you to Professor Gang Chen, Dr. Bachir El Fil, Natasha Stamler, and department librarian Claire Berman for your valuable feedback and support throughout this thesis. Thank you to Dan Gilbert, Wade Warman, and Josh Ramos for allowing me access to the LMP lab and teaching me valuable lessons in manufacturing. Finally, thank you to Adela Li and the rest of the MIT Device Research Lab for welcoming me so warmly as a UROP nearly one full year ago!

TABLE OF CONTENTS

List of Figures

List of Tables

1. Introduction

Access to clean water is one of the 17 Sustainable Development Goals outlined by the United Nations and is an increasingly prevalent issue around the globe. With worsening effects of climate change, global conflict, and socioeconomic disparities, more than 27% of people around the world lack consistent, reliable access to a clean water supply [1]. Atmospheric water collection presents a new potential solution to tackle this issue.

The MIT Device Research Lab is developing an adsorption-based atmospheric water-harvesting device, capable of producing drinkable water even in extremely dry environments. When exposed to the environment, even in relatively dry conditions (RH around 40% or less), water vapor will readily adsorb onto the coating until it reaches a saturated uptake value, an amount determined by the sorbent material and the environment's relative humidity. Current tests with this device use a thermal desorption process to extract water from the fins by applying heat to the system, which increases the localized vapor pressure at the surface of the fins' coatings. The water vapor collects onto a condenser, where it enters a liquid phase and can then be collected for use.

Another known method of desorption is with the use of pressure swings. This is a common practice currently used in the separation of gases, like in the collection of nitrogen from compressed air using crystalline materials such as zeolites as the adsorbent. With a pressure-based desorption method, bringing the pressure of the system down creates a similar effect as heating the sample up. The resulting pressure gradient- between the localized vapor pressure and the vapor pressure surrounding the substrate- initializes the release of the water vapor from the sample, making it possible to collect it with a condenser.

Using both thermal and pressure swing assisted desorption in tandem presents the potential for (1) the saturated water vapor to desorb at a much faster rate, and for (2) a less costly process as the combined method could require less energy to desorb the same amount of water (compared to either method on its own).

2. Background

2.1 Adsorption & Desorption Phenomena

Atmospheric water harvesting relies on the natural tendencies of certain substances to readily adsorb moisture in the air. Adsorption is the process by which this moisture in the air adheres onto the surface of a substance. This adhesion can happen through either physical or chemical attraction forces, but for water collection, this attraction is physical because it needs to be reversible in order to collect the water for use.

Desorption is the reverse process of adsorption, when the adsorbed molecules are released back into the environment. In the case of atmospheric water harvesting, the water vapor is released from the sorbent back into the air and then will condense onto a nearby surface into water droplets to be collected. The main types of desorption are thermal, pressure swing assisted, and chemical desorption.

Important environmental variables to consider in analyzing atmospheric water harvesting processes are the temperature and the relative humidity. Relative humidity is represented as a percentage and is calculated by:

$$Relative\ Humidity\ = \frac{Actual\ Vapor\ Density}{Saturation\ Vapor\ Density} \approx \frac{Actual\ Vapor\ Pressure}{Saturation\ Vapor\ Pressure}$$

From the temperature and relative humidity, one can find the actual and saturation vapor pressure of the surrounding environment. In a closed system at thermodynamic equilibrium, a vapor exerts a partial pressure that contributes to the whole pressure. The saturation vapor pressure is the maximum this pressure can be at a given temperature because it indicates that the maximum possible amount of water in the vapor state is present. The actual vapor pressure is this partial pressure exerted by the water vapor present in the air, and is thus representative of how much water vapor is currently present in the atmosphere. If the temperature (and thus the saturation vapor pressure) and relative humidity of a particular time is known, then the actual vapor pressure can be calculated using the relation shown above.

Atmospheric water harvesting relies on cycles of adsorption and desorption to collect this water vapor in the air. Currently, the common practice is to use thermal desorption, where

heating the substrate up will release the captured water, which is then released onto the surface of a condenser, and then stored as liquid water.

2.2 Mass transfer with Fick's Law

The mass transfer of the water vapor into and out of the sorbent can be modeled using Fick's first law of diffusion, which states that a diffused substance will move from areas of a higher concentration to areas of a lower concentration. To put differently:

$$J = -D \frac{d\varphi}{dx}$$

where J is the diffusion flux (amount / m^2 / s), D is the diffusion coefficient (m^2 / s), and $\frac{d\varphi}{dx}$ is the concentration gradient, in which φ is the concentration (amount / m^3) and x is position (m). With the assumption that the difference in vapor pressure is the linear driving force, this equation can be modified to express a relationship between the mass flux and the vapor pressure gradient (between the surrounding environment and localized right at the surface of the substrate):

$$m'' \propto D \cdot (P_v^* - P_v)$$

where m" is the mass flux (kg / m^2 / s), P_v^* is the localized vapor pressure (Pa), and P_v is the surrounding ambient vapor pressure (Pa).

In thermal desorption, the application of heat to the substrate effectively lowers the vapor pressure (increasing temperature increases the saturation vapor pressure, and at a given RH, this would have to lower the actual vapor pressure). The value of P_v does not change but due to the increase in P_v^*, the difference in vapor pressure increases with induces the mass flux of water vapor from the substrate out into the air.

2.3 Metal Organic Framework (MOF) UiO-66

Of many materials that exhibit potential for efficient adsorption and desorption cycles, metal organic frameworks (MOFs) are a compound that exhibit remarkable material properties for this particular application. These materials, in addition to zeolites and silica gels, are porous

crystalline materials that provide an ideal interface for adsorption of water vapor. They are particularly desirable for its ability to adsorb water vapor even in fairly dry conditions, when RH is below 40%. This expands the potential reach of this technology to assist those living in climates that are likely more prone to clean water scarcity. MOFs are also highly adjustable in the way they are made, so they can be customized to mitigate different obstacles with the adsorption-desorption collection process, such as a low uptake value or a high energy requirement to desorb.

UiO-66 is a zirconium-based MOF and is characterized with particularly large pore volumes and thus a large water uptake capacity. Figure 2-1 by Cui *et al.* [8], shows the water uptake data for UiO-66 vs the relative humidity in relation to other MOFs commonly used as sorbents in water harvesting. For these desirable material properties, UiO-66 is the selected sorbent used in this experiment.

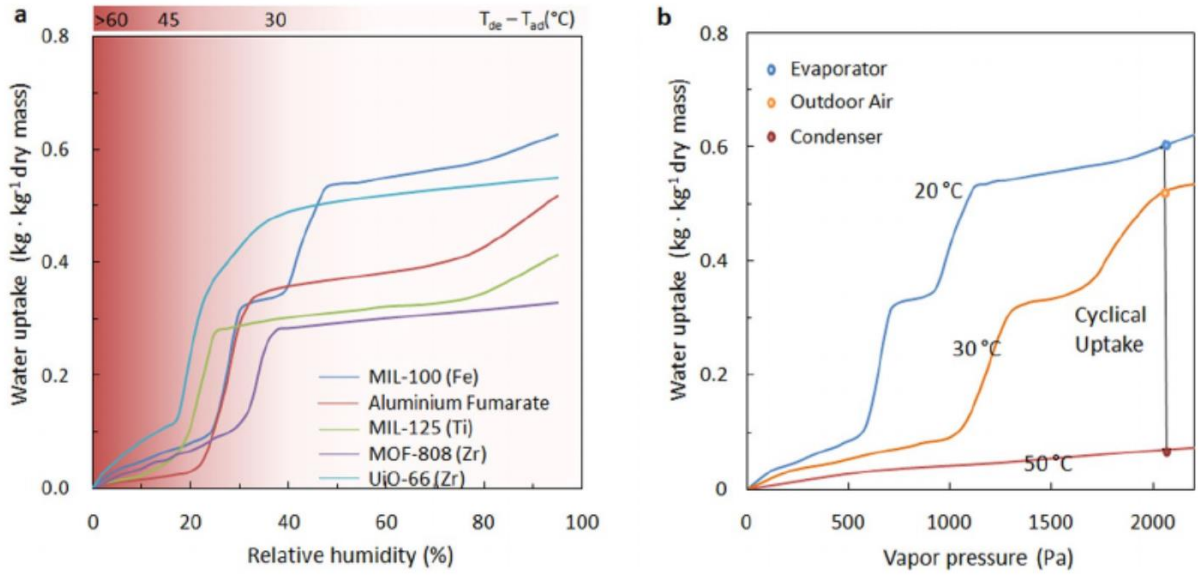

Figure 2-1: Uptake data of multiple common sorbents including UiO-66 [8]

3. Methods for Experiment

In proposing that incorporating pressure swings is a viable alternative to purely thermal desorption for atmospheric water harvesting, the first step is to compare the desorption rates and thus its ability to release captured water vapor more quickly. Using the metal organic framework UiO-66 as my sorbent, I conducted three separate cases: (A) using purely thermal desorption with a heated pad set to 140°C, (B) using purely depressurized desorption with a bell jar and pump, and (C) using both methods in tandem. In particular, I measured the changes in mass of the system with time throughout its desorption phase, from which I can show the relative desorption rates and the time constants of each case.

To prepare the samples of UiO-66 for the experiment, they were first dried in a furnace overnight set at 120°C. This preparation desorbed the samples to ensure a good reading of its dry mass (i.e. there was no water vapor adsorbed in the material). I measured three equal samples with a dry mass of approximately 9.75 grams, which I then left sealed in a jar until each experiment was ready to begin to ensure minimal adsorption and subsequent mass gain. For each case, the UiO-66 sample was transferred to a small glass dish, measured again, and then left open to the environment for one hour as the adsorption phase.

Both adsorption and desorption experiments took place in a fume hood, in which I took note of the relative humidity and temperature data, which remained relatively consistent throughout all three experiments. This data was collected in table 3-1, from which I calculated the average that I reference in my analysis. Each sample stayed uncovered in the fume hood for one hour and after undergoing an adsorption cycle, I recorded the new mass of the saturated substrate. One hour was not enough for the sample to reach its full saturated adsorption state but this adsorption time and thus its uptake for each sample was maintained the same. From this measurement, the uptake of the sample is calculated using:

$$Uptake = \frac{Mass\ of\ water\ adsorbed\ (g)}{Dry\ mass\ of\ sorbent\ (g)}$$

The uptake represents the capacity of how much water a material can adsorb (in g/g = unitless) in a given sample and varies with relative humidity, as shown previously in figure 2-1.

The sample is now ready for its respective method of desorption to extract this adsorbed water.

3.1 Case A: Purely thermal desorption

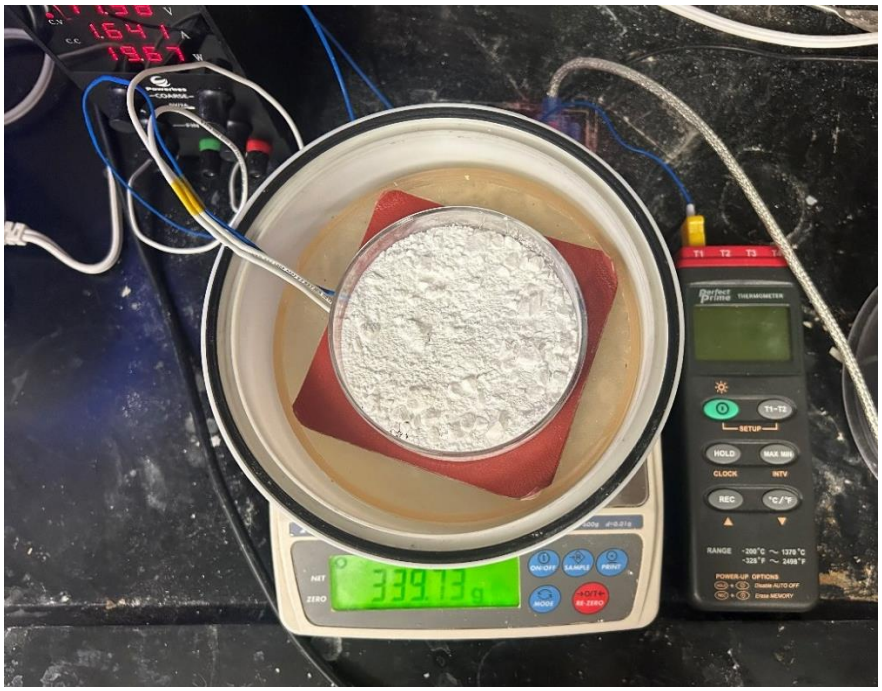

Figure 3-1: Experiment set-up for case A (thermal desorption).

Case A tested the standard thermal desorption method. The dish of the saturated UiO-66 sample was heated at 140°C using the red pad as shown in Figure 3.1, which was connected (via the two white wires) to a power supply in the fume hood providing approximately 12 V and 20 W throughout the experiment. The translucent yellow dish was an extra part I measured and printed using high temperature resin on an SLA 3D printer to protect the bell jar's plastic infrastructure from the heating pad. To read out and maintain constant temperature of the sample dish, the blue wire was a thermocouple connecting a data acquisition (DAQ) device and contacted the system on top of the center of the red pad below the sample dish.

In reflection after conducting experiments, an important note to make with this set-up is that the temperature in the sorbent is not the same as the temperature of this thermocouple reading. Additionally, because the thermocouple was wired beneath the glass dish containing the sorbent, the dish was also not sitting completely flat on the heating pad. Using a simple thermal resistance network, the system can be modeled as two thermal resistors in series, one of which is for the glass dish and the other represents a lumped resistance for the errors alluded to above.

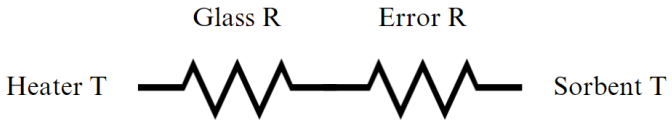

Figure 3-2: Simple thermal resistance network representation

Using 1.05 W/(m K) [13] as the thermal conductivity (k) for glass, I took sample measurements with thermocouples in the sorbent with the heating pad turned on. The "Heater T" in figure 3-2 was obtained through a thermocouple placed between the heating pad and the container, and is thus representative of the container surface temperature. Using the thermal resistance analogy and that $= \frac{\Delta T}{Q/A} = \frac{L}{k}$, I concluded that 82°C was a reasonable characteristic temperature for the sorbent for the cases in which the heating pad was in use and set to 140°C.

3.2 Case B: Pressure swing assisted desorption

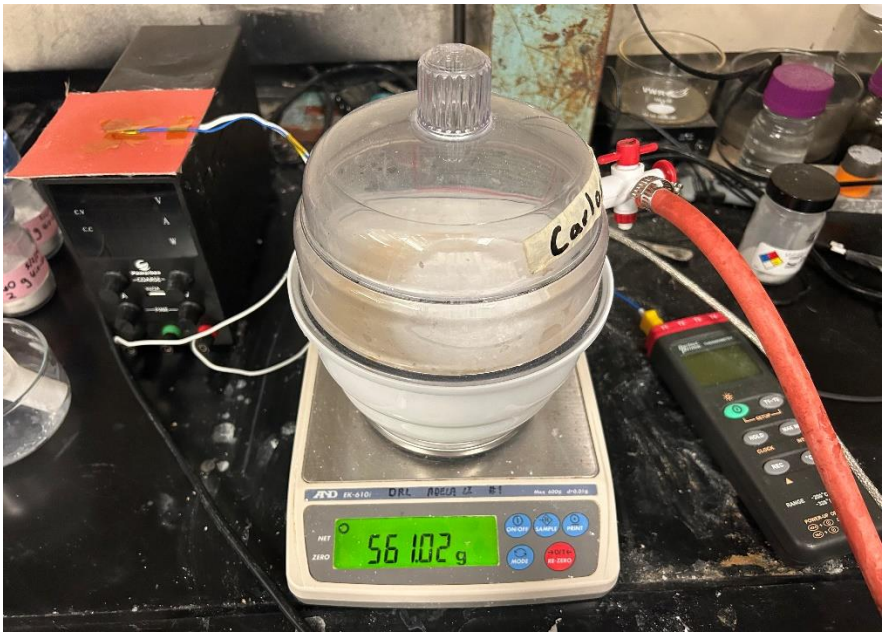

Figure 3-3: Experiment set-up for case B (depressurized desorption)

In case B, I used a plastic bell jar top and a pump (located just outside of the fume hood) to create the pressure drop. The pressure swing assisted desorption experiments introduced a new source of uncertainty in the mass flux because of the initial relatively large drop in mass when the air inside is being pumped out and the system approaches equilibrium. To help offset this

uncertainty, I ran the pump and set-up a few times without any sample of the UiO-66 sorbent inside. This mass vs. time data for one of these trials is shown below in figure 3-4.

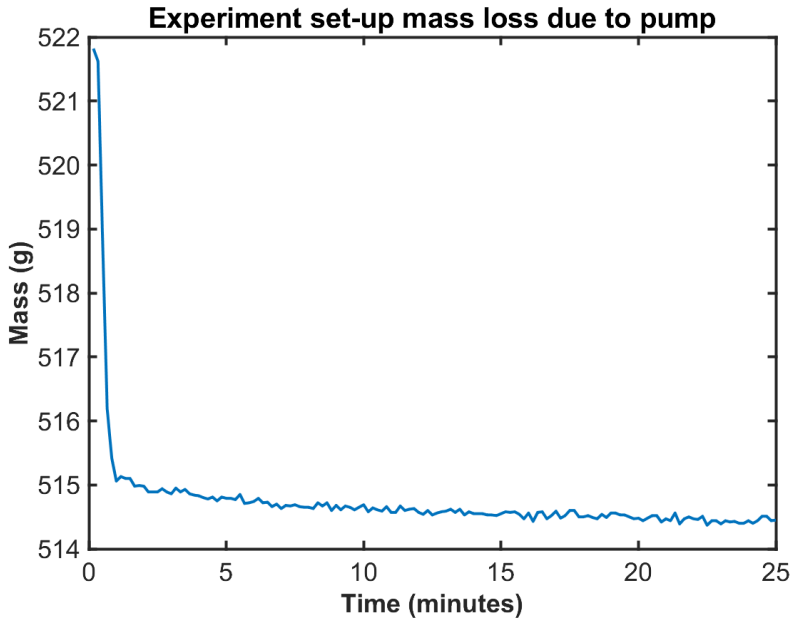

Figure 3-4: Test run of the bell jar and pump with no samples inside.

In my analysis, I subtracted this data set (and the steady state value for any points beyond 25 minutes) to offset the change in mass due to air being pumped out of the system. What remained was solely the changes in mass due to the desorption process.

3.3 Case C: Thermal & PSA in tandem

(a) 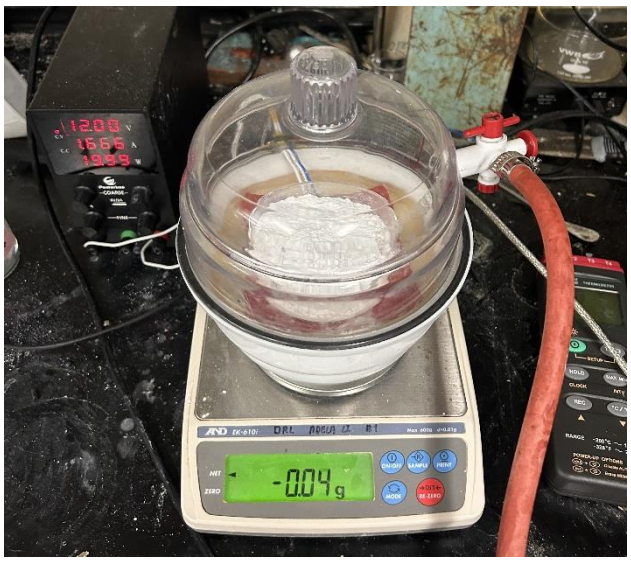 (b) 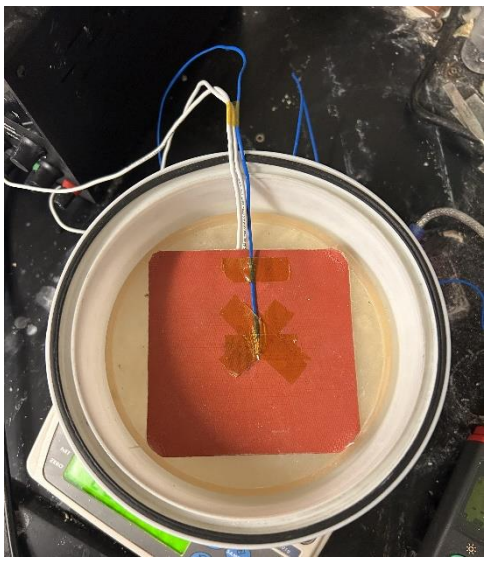

Figure 3-5: Experimental set-up for case C (Thermal & PSA in tandem).

Setting up case C came with the additional challenge of keeping everything airtight while being able to feed the three wires (two associated with the heating element, one for the thermocouple) from inside the bell jar to outside without breaking the seal. To accomplish this, I lined the inner rim of the bell jar with a 1/8" gasket and used Kapton tape to secure the wires together so that they would snugly fit into the gap in the ring. With the bell jar placed on top and the pump on, I also used an additional small length of the gasket to seal the area around the wires. This piece of gasket was held in place by the suction through the gap due to the pump.

In each of the three cases, the data from the A&D scale was connected to a laptop that ran the WinCT RsWeight software. With this configuration, the software recorded the mass measurement at a rate of one sample every ten seconds and plotted it in real time, so that I could easily identify when the system appeared to have reached steady state (and was thus fully desorbed).

3.4 Environmental parameters

Temperature and relative humidity played a large role in these experiments, so it was important to keep track of them throughout the experiment. Since these values did not vary too drastically within the fume hood where the tests were conducted, I used the average values over the course of the day in my analysis.

Time	Temperature (°C)	Relative Humidity (%)
10:51 AM	23.8	38
1:09 PM	24.3	39
2:15 PM	24.1	40
4:58 PM	24.3	40
7:02 PM	24.0	40
9:06 PM	24.2	40
10:48 PM	23.7	37
average	**24.1°C**	**39 %**

Table 3-1: Temperature & Relative Humidity measurements throughout the day.

Taking these average values as the representative temperature and relative humidity for this experiment, the saturated pressure at 24.1°C is 3004 Pa [13] and thus the resulting ambient vapor pressure is 1172 Pa.

4. Results

4.1 Measurements

	Case A: Thermal	Case B: Pressure	Case C: In tandem
Dry mass (g)	9.67	9.69	9.65
Mass after 1 hr. adsorption (g)	11.08	11.12	11.10
Mass after desorption (g)	9.98	10.01	9.67
Uptake (g of water/g of dry)	0.146	0.148	0.150

Table 4-1: Mass measurement data from cases A, B, C.

From the data above, the uptake of each sample can be calculated using:

$$Uptake = \frac{Mass\ of\ water\ adsorbed\ (g)}{Dry\ mass\ of\ sorbent\ (g)}$$

Seeing how this uptake decreases with time over the course of the experiment is useful in characterizing its desorption rate; the faster the uptake of the sorbent decreases, the faster the device can collect water for use.

4.2 Uptake vs. time plots

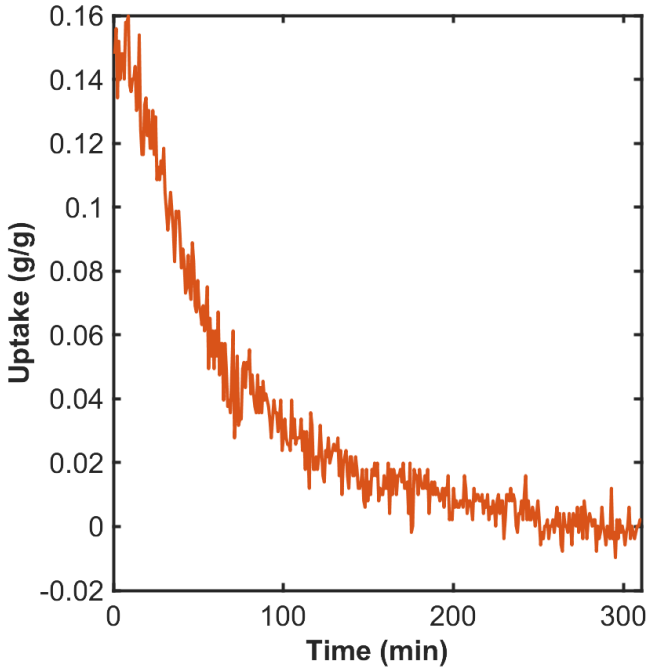

Figure 4-1: Uptake vs. time data for case A (purely thermal desorption at 140°C)

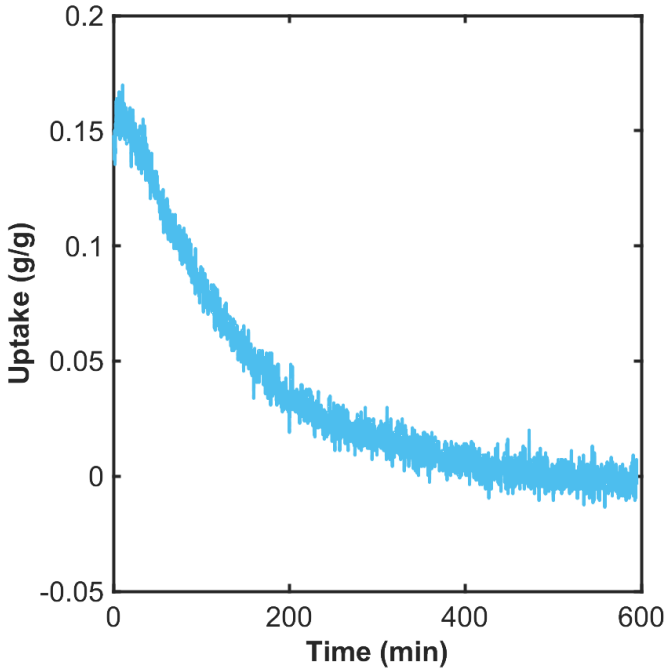

Figure 4-2: Uptake vs. time data for case B (purely depressurized desorption)

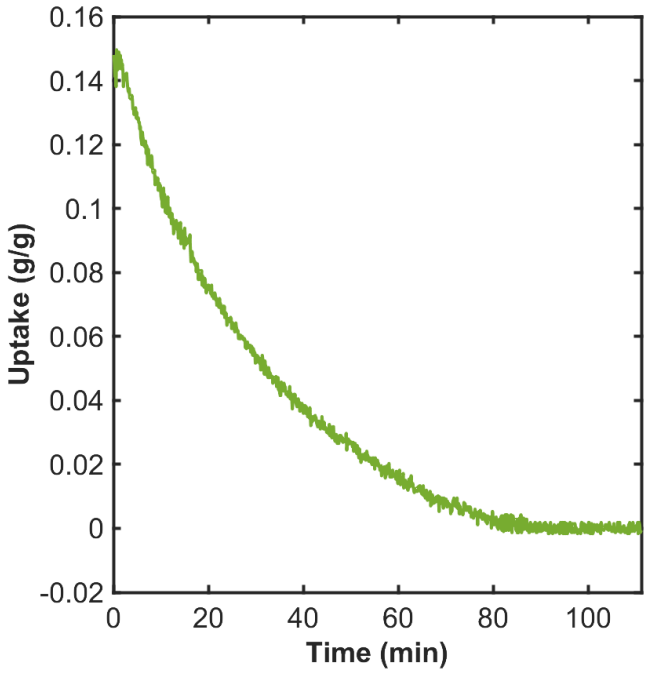

Figure 4-3: Uptake vs. time data for case C (thermal and depressurized in tandem)

5. Discussion of Results

5.1 Decrease in uptake over time

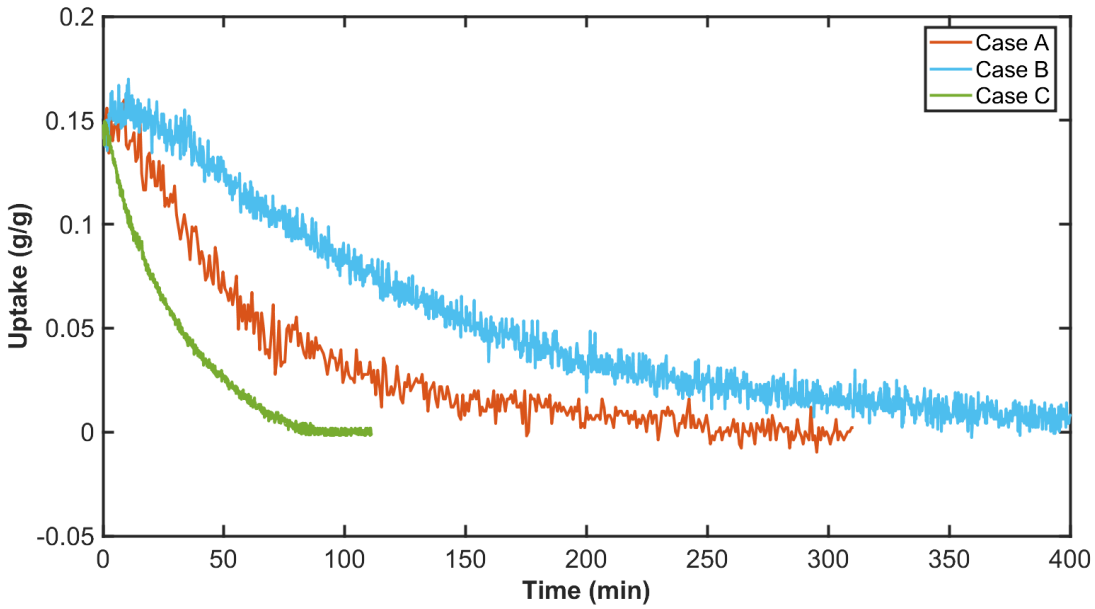

Figure 5-1: Uptake vs time of cases A, B, C

The uptake data collected for the three cases laid over each another in one plot is shown above in figure 5-1. At a glance, one can qualitatively see how much faster case C- where both temperature and pressure swings are working in tandem- are much more effective than either method at work desorbing on its own.

5.2 Time Constants

Finding the time constant for each set of data allows us to quickly compare the relative rates of desorption of the three cases. One time constant is the amount of time passed by which the sample will have decreased to 1/e ≈ 36.8% of its initial value. These time constants (τ) for each scenario are shown on their respective plots in figures 5-2, 5-3, and 5-4 below.

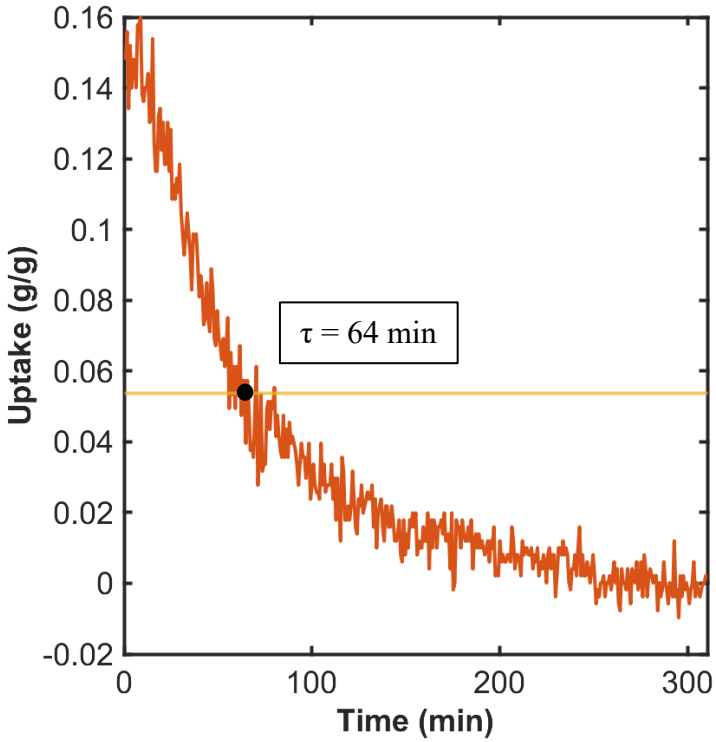

Figure 5-2: Time constant for case A = 64 min.

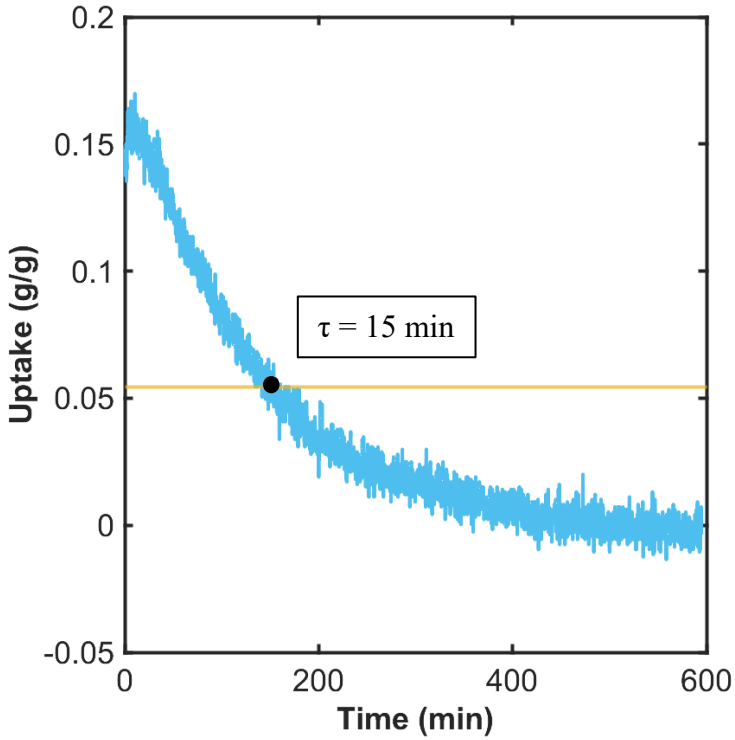

Figure 5-3: Time constant for case B = 152 min.

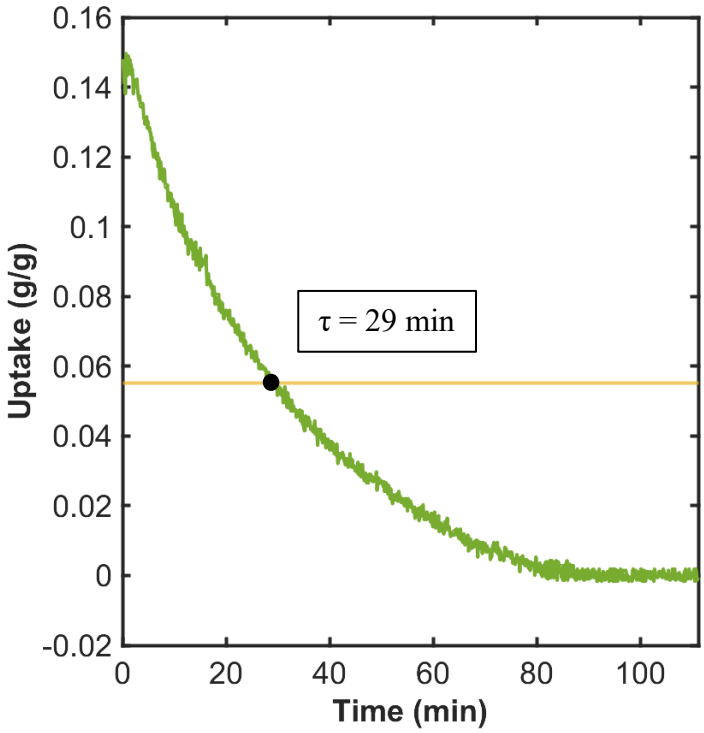

Figure 5-4: Time constant for case C = 29 min.

Using the time constants for the three cases, the combination method proved to be the fastest; it was more than twice as fast as the purely thermal desorption method and more than five times as fast as a purely depressurized method.

5.3 Limitations of experimental set-up

As alluded to in the Methods for Experiment section (chapter 3), this experimental set-up works as a validation experiment to prove pressure swing assisted desorption is a worthwhile method to explore for atmospheric water harvesting. However, there are many experimental uncertainties that arise from the simplicity of this set-up.

Firstly, because of the placement of the thermocouple on the heating pad below the sorbent, the glass dish didn't have the best contact possible with the heating element. This led to uneven heating throughout the sorbent, possible inaccuracy in the actual sorbent temperature, and inconsistency between experiments. However, in real applications of this method with the current water collection device, the sorbent is applied as a thin coating to metal fins, which are

then assembled in a structure holding them parallel to each other. These inaccuracies would be mitigated in this scenario and in this experiment, has not hindered the results to the point of the overall, relative relationships being inaccurate.

In order to track the changes in mass of the water adsorbed, the entire system was placed on a scale and the mass was recorded over time. Especially with cases B and C, where a pump was involved, there were many changes in mass due to the removal of air. The error from this change was accounted for by subtracting the data from a dummy run of the system with no sample inside (just the bell jar enclosure and relevant attachments). Another possible source of error came from the tube that connects the bell jar on top of the mass balance to the pump outside of the fume hood. Caution was taken to ensure there was minimal force applied from this component onto the scale, but naturally, because the tube provides another structural point of contact, the mass balance reading can alter if the tube shifts at all in the duration of the run. Two options of changing the experimental set-up that would avoid this are (1) obtain a much bigger bell jar or vacuum chamber that can fit a mass balance inside or (2) to monitor the water content itself rather than mass changes. Option 2 can only be achieved by monitoring the process more holistically by including the condensation phase of the collection cycle.

5.4 Conclusions

As seen qualitatively through the graphs and quantitatively through the time constants, the combined method with thermal and pressure swing assisted desorption proves to be a much faster and more effective method of desorption than the current practice of using solely thermal desorption. The solely thermal method had a time constant of 64 minutes, the solely depressurized method had 152 minutes, and the combined method had 29 minutes, a sizable decrease in time and thus a much higher rate of desorption. As a proof of concept experiment, this data proves how a combined method is a worthwhile endeavor to pursue in researching methods of atmospheric water collection by showing it has a smaller time constant and faster desorption rate.

6. Future Work

6.1 Design of Vacuum Chamber

To further validate that using pressure swing assisted desorption is a viable and worthwhile method of atmospheric water harvesting, the procedure needs to be tested with a small test unit of the device containing coated fins and in a much more controlled environment. Below is my design for a vacuum enclosure that eliminates several uncertainties introduced by the simplicity of the set-up in the "proof of concept" experiment in this thesis. The structure is a 12" x 8.75" x 9.46" box made of a combination of aluminum, SLA 3D-printed plastic, and polycarbonate components.

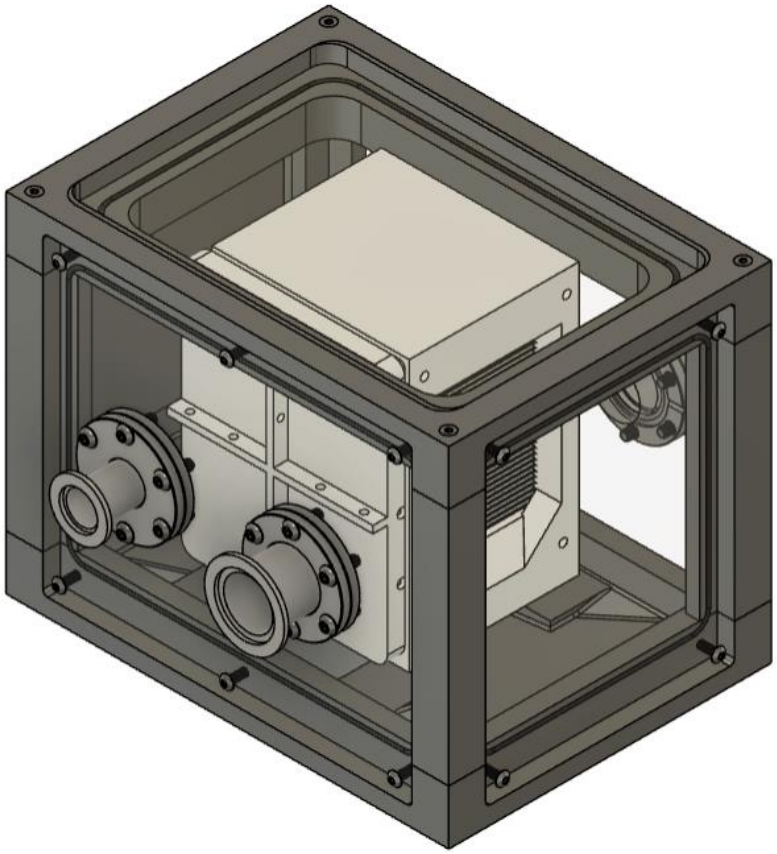

Figure 6-1: Vacuum chamber CAD for further pressure swing validation testing.

Three crucial design requirements of this enclosure is (1) that it is airtight and is capable of pulling the system down to an extremely low pressure, (2) that the enclosure can be opened and closed repeatedly to remove the device in between experiments, and (3) that several inputs and outputs can be attached without sacrificing its vacuum capabilities.

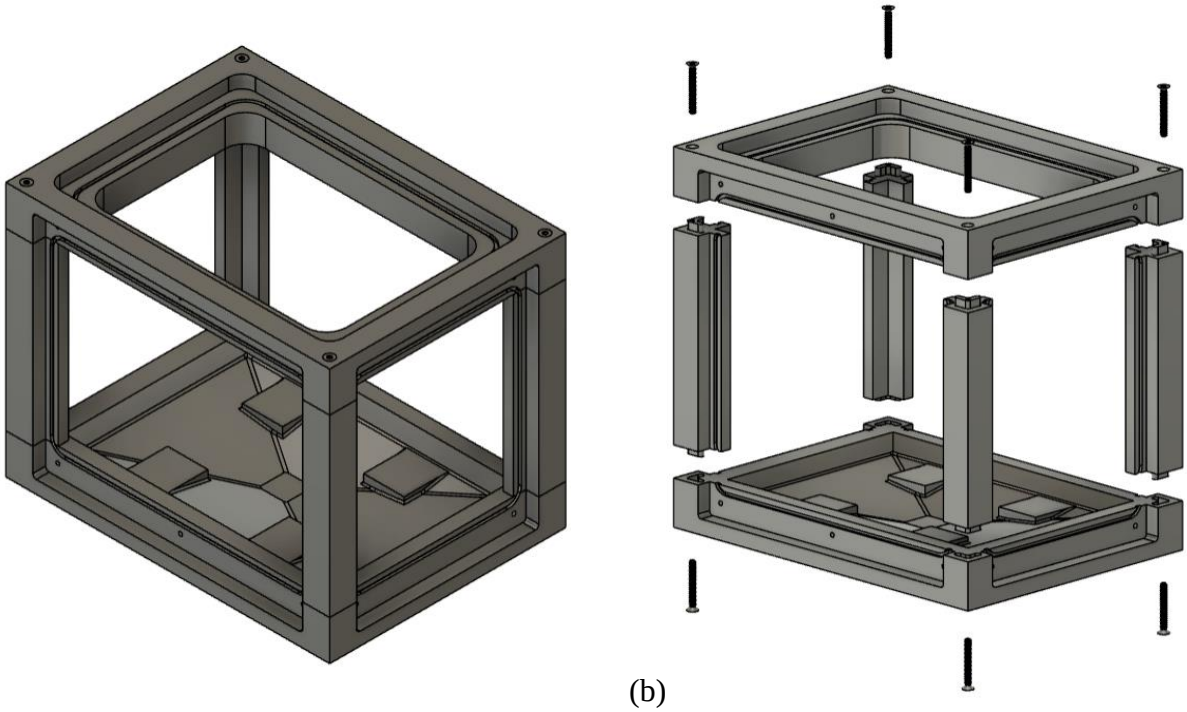

(a) (b)

Figure 6-2: (a) Assembled and (b) exploded view of the chamber's skeleton structure

Figure 6-3: Exploded view of enclosure's top components and close-up of O-ring groove.

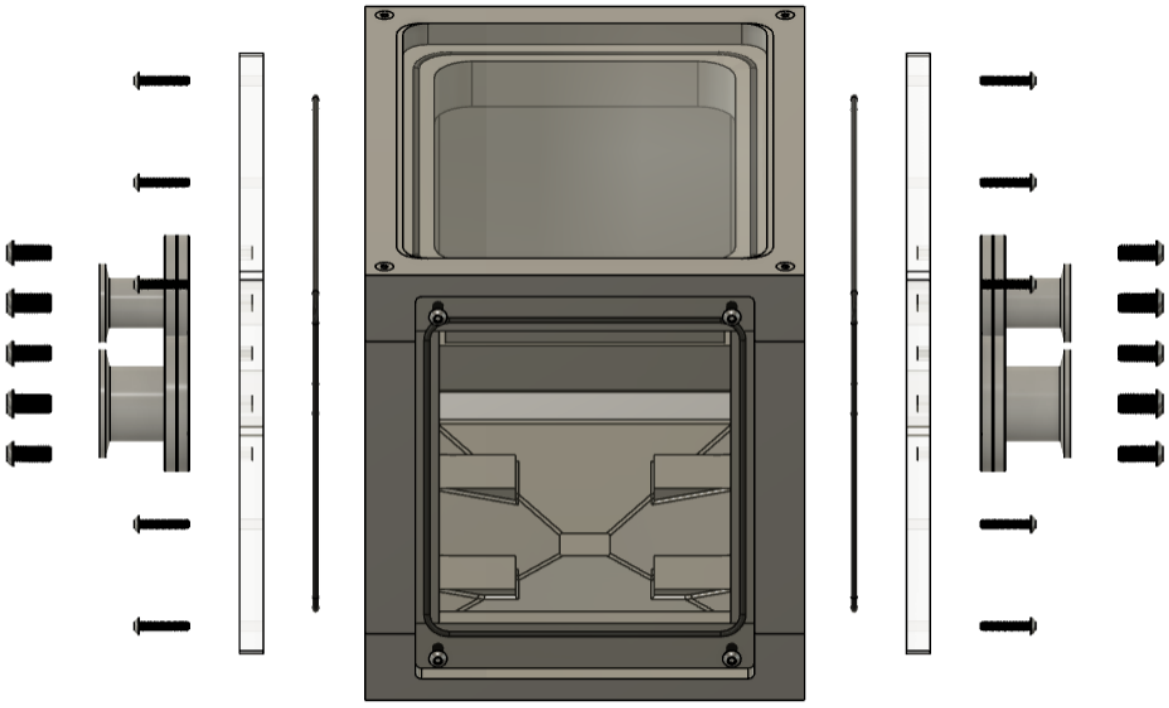

Figure 6-4: Exploded view showing the enclosure's front and back side components.

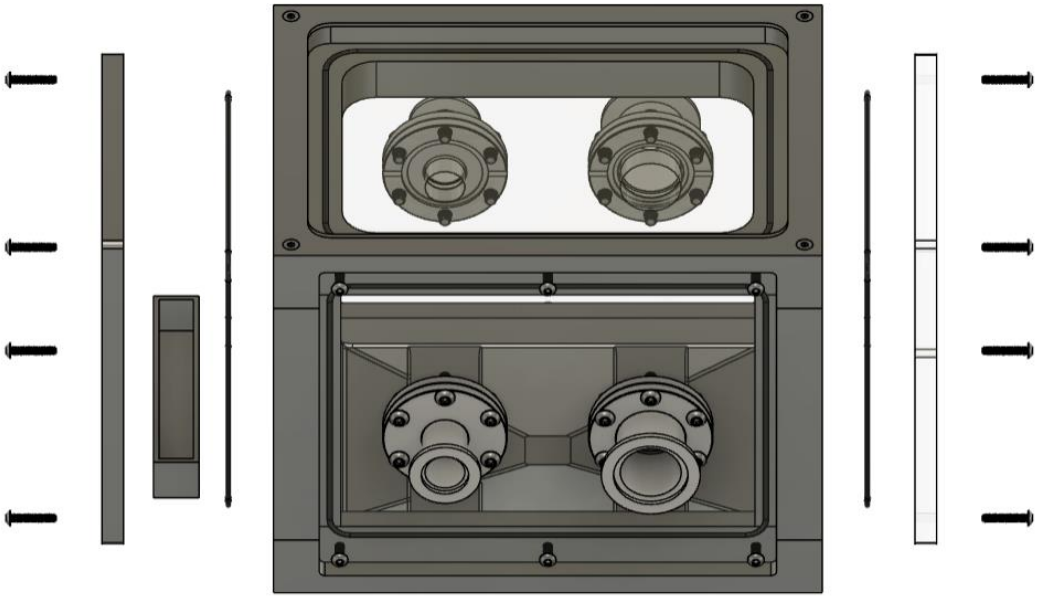

Figure 6-5: Exploded view showing the enclosure's left and right side components.

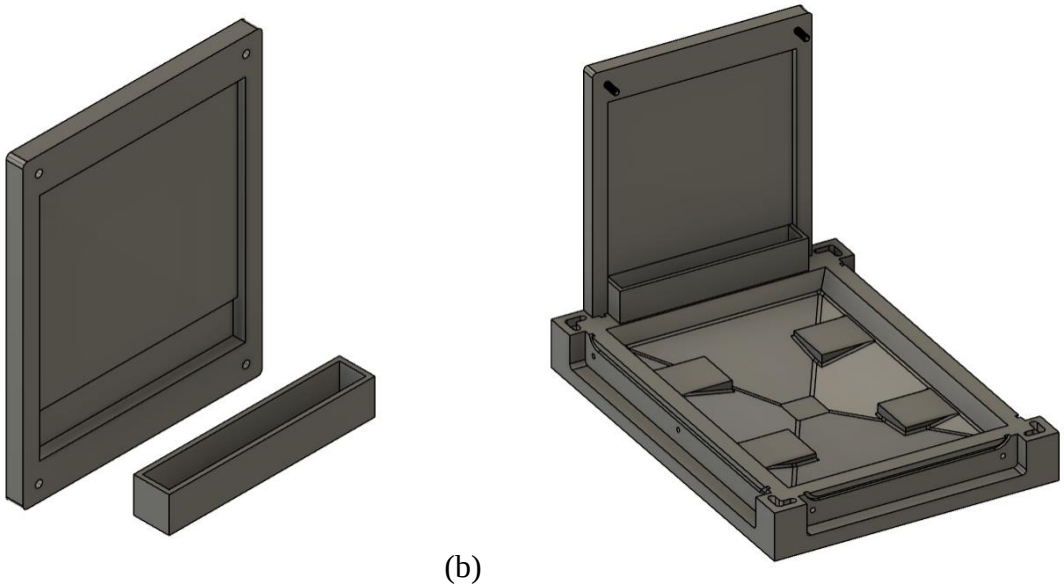

(a) (b)

Figure 6-6 : (a) Condenser wall and bin. (b) Condenser wall in relation with bottom.

Flange adapters provide the interior with access to a pump, power, and wired sensors without sacrificing its vacuum integrity. As displayed in figures 6-1, 6-4, and 6-5, there are four total flange adapters: a CF40-KF25 and CF40-KF40 on each of the front and back walls. The two CF40-KF40 adapters connect to KF40 flanged electrical feedthroughs, one of which connects to several thermocouples and the other supplies powers to the heating component of the device test unit. The front CF40-KF25 adapter connects to the pump used to draw a vacuum inside the chamber, and the back CF40-KF25 adapter connects to a pressure transducer in order to monitor the interior pressure throughout the experiment.

The top and bottom frames and the condenser wall (shown in figure 6-6) of the enclosure are manufactured from multipurpose 6061 aluminum. The bin of the condenser is 3D printed and can be easily removed from the structure in order to measure the amount of water collected in a cycle. The four columns are SLA 3D-printed using rigid 10K resin because of the detailed groove design necessary for the o-rings. The four clear walls are thick polycarbonate sheets water jetted to include the correct outlines and holes. At the interface of each wall and the skeleton structure, there is a 1/8” gasket to ensure a good, airtight seal. As show in the figures above, many screws attach the components to each other and additionally are reinforced with the vacuum-grade epoxy to minimize any gas leakage at those entry points.

6.2 Outgassing and leakage considerations

There are two primary sources of gas leakage into the chamber. The first is that there can be gaps between the different components after assembly of the enclosure. To mitigate this, when assembling the skeleton structure, there are specific geometries on the interface of the columns and the top and bottom frames (which are visible in figure 6-2b). These ensure a tight fit and that the components can only be assembled in one configuration. A vacuum grade seal epoxy is also applied at that interface before the screws tighten the components together.

The second source is due to outgassing characteristics of the material, where previous trapped gaseous substances in the material can slowly desorb and diffuse into an area of lower pressure, e.g. the interior of this vacuum enclosure. Referencing the material options to a NASA outgassing database, I concluded that the materials I selected should be appropriate for my use [15]. This database collected information on the outgassing data for materials intended for spacecraft use and outlines that appropriate materials should have a maximum total mass loss (TML) of 1.0% and a maximum collected volatile condensable material (CVCM) of 0.10%.

	TML (%)	CVCM (%)
Requirement (≤ this value)	1.0	0.10
Aluminum	0.10	0.01
Polycarbonate	0.2	0.04
SLA 3D printed (PP)	0.34	0.08
Vacuum epoxy	0.19	0.01

Table 6-1: Outgassing characteristics of materials used in enclosure design

As all materials have a TML and CVCM value within the reference requirement, gas leakage into the chamber due to any outgassing phenomena of the materials should be minimal.

6.3 Experimental approach

After the vacuum enclosure has been validated that it can pull a vacuum and reach a reliably steady state, a similar outline of experiments can be performed. To confirm that pressure-swing assisted desorption in tandem with thermal desorption is the best method, the set-up must first be tested with solely thermal desorption, then solely depressurized desorption, then

a combined procedure with the same settings. The results from the solely depressurized desorption experiment should be more effective than the parallel results in this paper, as the pressure can be drawn to a much lower to a near (if not complete) vacuum). After this initial validation of the method, additional tests can help determine what settings of the combined method can achieve the same results as the current testing methods of the device. In particular, what is the lowest temperature the heating element in the combined method can be set to such that it can achieve the same results as the purely thermal desorption method? Does this present any desirable advantages in power usage, energy efficiency, or cycle time?

7. Bibliography

[1] United Nations Statistics Division, 2023, “The Sustainable Development Goals Report”, from https://unstats.un.org/sdgs/report/2023/

[2] Zhou, X., Lu, H., Zhao, F., and Yu, G. 2020, “Atmospheric Water Harvesting: A Review of Material and Structural Designs”, ACS Materials Letters, from https://pubs.acs.org/doi/10.1021/acsmaterialslett.0c00130

[3] Yang, K., Pan, T., Lei, Q., Dong, X., Cheng, Q., and Han, Y., 2021, “A Roadmap to Sorption-Based Atmospheric Water Harvesting: From Molecular Sorption Mechanism to Sorbent Design and System Optimization”, Environmental Science & Technology, from https://pubs.acs.org/doi/10.1021/acs.est.1c00257

[4] The Engineering ToolBox, 2018, “Air - Diffusion Coefficients of Gases in Excess of Air “, from https://www.engineeringtoolbox.com/air-diffusion-coefficient-gas-mixture-temperature-d_2010.html

[5] Shi, W., Guan, W. Lei, C., and Yu, G., 2022, “Sorbents for Atmospheric Water Harvesting: From Design Principles to Applications”, from https://onlinelibrary.wiley.com/doi/full/10.1002/anie.202211267

[6] Kim, H., Yang, S., Rao, S., Narayanan, S., Kapustin, E., Furukawa, H., Umans, A., Yaghi, O., and Wang, E., 2017, “Water harvesting from air with metal-organic frameworks powered by natural sunlight”, from https://www.science.org/doi/10.1126/science.aam8743#core-R1

[7] Hanikel, N., Prévot, M.S. and Yaghi, O.M., 2020, “MOF Water Harvesters”, Nature Nanotechnology, from https://www.nature.com/articles/s41565-020-0673-x#Sec3

[8] Cui, S., Qin, M., Marandi, A., Steggles, V., Wang, S., Feng, X., Nourar, F., and Serre, C., 2018, “Metal-Organic Frameworks as advanced moisture sorbents for energy-effcient high temperature cooling”, Scientific Reports, from https://www.researchgate.net/publication/328316676_Metal-Organic_Frameworks_as_advanced_moisture_sorbents_for_energy-efficient_high_temperature_cooling/link/5fb563ce92851c2994e4cb64/download

[9] Ghosh, P., Colón, Y., and Snurr, R., “Water adsorption in UiO-66: the importance of defects”, Chemical Communications, **77**, from https://pubs.rsc.org/en/content/articlelanding/2014/cc/c4cc04945d#cit10

[10] Hossain, M., and Glover, T.G., 2019, “Kinetics of Water Adsorption in UiO-66 MOF”, from https://pubs.acs.org/doi/10.1021/acs.iecr.9b00976

[11] Winarta, J., Shan, B., Mcintyre, S., Ye, L., Wang, C., Liu J., and Mu, B., 2020, “A Decade of UiO-66 Research: A Historic Review of Dynamic Structure, Synthesis Mechanisms, and Characterization Techniques of an Archetypal Metal–Organic Framework”, from https://pubs.acs.org/doi/10.1021/acs.cgd.9b00955

[12] Bůžek, D., Adamec, S., Lang, K., and Demel, J., “Metal-organic frameworks vs. buffers: case study of UiO-66 stability”. Inorganic Chemistry Frontiers, **3**. from https://pubs.rsc.org/en/content/articlelanding/2021/qi/d0qi00973c

[12] Glass thermal conductivity https://www.engineeringtoolbox.com/thermal-conductivity-d_429.html

[13] The Engineering ToolBox, 2003, “Solids, Liquids, and Gases - Thermal Conductivities”. from https://www.engineeringtoolbox.com/water-vapor-saturation-pressure-d_599.html?vA=140&units=C#

[14] The Engineering ToolBox, 2018, “Air-Diffusion Coefficients of Gases in Excess of Air.” from https://www.engineeringtoolbox.com/air-diffusion-coefficient-gas-mixture-temperature-d_2010.html

[15] National Aeronautics and Space Administration, 1993, “Outgassing Data for Selecting Spacecraft Materials”, from https://outgassing.nasa.gov/outgassing-data-table